Wind and Structures, Vol. 16, No. 4 (2013) 393-409

DOI: http://dx.doi.org/10.12989/was.2013.16.4.393

Wind-induced response and loads for the Confederation Bridge. Part II: derivation of wind loads

Bilal Bakht *[1], J. Peter C. King[2] and F. M. Bartlett[3]

[1]*Ministry of Transportation and Infrastructure, KAMLOOPS BC, Canada*
[2]*Boundary Layer Wind Tunnel Laboratory, University of Western Ontario, London ON, Canada*
[3]*Department of Civil and Environmental Engineering, University of Western Ontario, London ON, Canada*

(Received September 7, 2011, Revised March 25, 2012, Accepted May 17, 2012)

Abstract. This paper uses ten years of on-site monitoring data for the Confederation Bridge to derive wind loads and investigate whether the bridge has experienced its design wind force effects since its completion in 1997. The load effects derived using loads from the on-site monitoring data are compared to the load effects derived using loads from the 1994 and 2009 wind tunnel aerodynamic model tests. The research shows, for the first time, that the aerodynamic model-based methodology originally developed in 1994 is a very accurate method for deriving wind loads for structural design. The research also confirms that the bridge has not experienced its specified (i.e., unfactored) wind force effects since it was opened to traffic in 1997, even during the most severe event that has occurred during this period.

Keywords: full-scale, long-span, RMS accelerations, load effects, aerodynamic damping, wind tunnel testing, full-aeroelastic model, mode shape, frequency

1. Introduction

Modern bridge codes recommend that wind tunnel tests be carried out for long-span or wind-sensitive bridges to determine design wind loads. For example, the Canadian Highway Bridge Design Code (CHBDC) specifies that wind-tunnel testing be carried out for bridges that have individual spans greater than 125 m or are otherwise wind sensitive (CSA 2006). British Standard BS 5400 recommends wind-tunnel testing to account for the lateral, vertical and torsional dynamic effects for bridges with spans greater than 200 m (BSI 2009). The American Association of State Highway and Transportation Officials (AASHTO) Load and Resistance Factor Design (LRFD) Specification requires in-depth evaluation of potential aeroelastic instabilities using wind-tunnel tests of any bridge or structural component with a span/depth or span/width ratio greater than 30 (AASHTO 2004).

Traditionally, section models are used to assess the behaviour and determine the design wind loads of a long-span bridge. Limitations to this approach have been recognized for bridge superstructures with varying deck cross section, plan geometry or tower height (e.g., King 1999). Full-aeroelastic models that replicate the geometry, stiffness and mass properties of the entire

∗Corresponding author, Dr., E-mail: Bilal.Bakht@gov.bc.ca

bridge provide a promising alternative to assess the wind loads on bridges with properties that vary along the span length.

The load effects on the bridge produced in a severe wind storm have static and dynamic components, as illustrated in Fig. 1 (King *et al*. 1994). The static load components are produced by the mean wind and are defined using force coefficients that are generally measured from section model tests. The dynamic components are the inertial loads caused by the dynamic movement of the bridge vibrating in its natural modes; usually only the modes with the longest periods are significant. The bridge response due to the combined effect of the static and dynamic wind loads can be expressed in terms of a variety of structural actions including forces, bending moments, stresses, displacements or accelerations. The form of such responses has been illustrated by Davenport (1964, 1979, 1988) and expressed as

$$\hat{R} = \overline{R} + g\,R_{t_d} \tag{1}$$

where $\hat{R}$ is the peak response, $\overline{R}$ is the mean response, g is a statistical peak factor, usually in the range 3–5, and R_{t_d} is the total dynamic response as defined in detail in the companion paper.

It has been suggested that to properly account for the response of long span bridges it is necessary to include as many as 20 modes of vibration in an equivalent wind load model (Scanlan 1987). Davenport and King (1984) have taken a different approach whereby a load model consisting of the minimum number of symmetric and asymmetric modes in three degrees of freedom are sufficient to capture the important load effects for design purposes. This approach was adopted for the Sunshine Skyway Bridge and a methodology was developed using section model test data to derive wind loads for the bridge design (Davenport and King 1984). Keeping in view the limitations of this approach for bridges with varying deck cross section, this methodology was

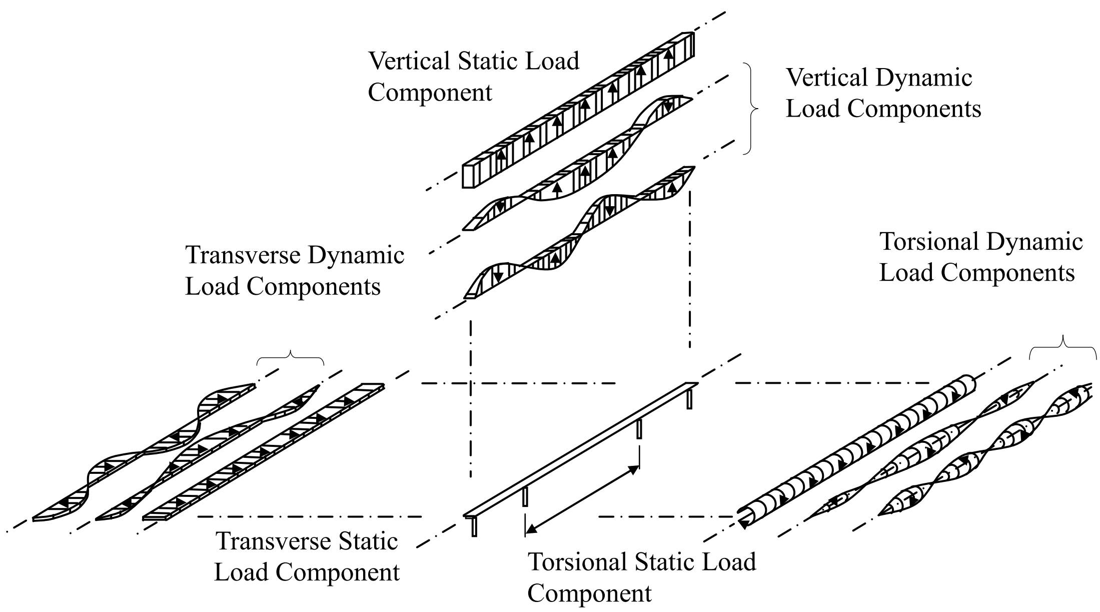

Fig. 1 Distributed Wind Load Components (adapted from King *et al*. 1994)

further developed to use full-aeroelastic model test data to derive wind loads for the Confederation Bridge design (King *et al*. 1994, King *et al* 1995).

This methodology is used to derive wind loads for the Confederation Bridge from the on-site monitoring data described in the companion paper to examine, for the first time, the appropriateness of the wind loads specified for the bridge design. The equivalent full-scale static force coefficients determined from the section model tests in 1994 are compared to the full-scale coefficients determined from the in-place monitoring data. The dynamic load effects due to wind derived using aeroelastic wind-tunnel models, tested in 1994 and 2009, and on-site monitoring data are compared to investigate the sensitivity of the methodology and results obtained for the dynamic wind loads used for the design of the bridge. Finally, the peak bending moments used for the bridge design are compared to the peak bending moments predicted using loads derived from the in-place monitoring data to investigate if the bridge has actually experienced its design moments since its completion in 1997.

2. Wind loads from the on-site monitoring data

The analyses of the measured static and dynamic bridge responses have been presented in the companion paper. A parabolic fit to the tiltmeter data, proposed by Bruce and Croasdale (2001), was used to determine the static drag coefficients for comparison with the original design values. Static lift coefficients are not addressed because the on-site monitoring program was not designed to capture force effects in the vertical direction. Therefore, mean static bending moments determined from the 2009 wind tunnel tests results are added to the dynamic effects determined from regression analysis of the on-site monitoring data to obtain the peak bending moments for comparison with the original design values. The derivation of static drag coefficients and dynamic wind loads is presented in the following sections.

2.1 Static drag coefficients

The horizontal winds applied to the superstructure and pier shafts of the Confederation Bridge cause the tops of the piers to deflect laterally, which is measured by tiltmeters attached to the pier shafts (Brown 2007). The measured mean tilts are due to the mean wind load acting over a 250 m length of bridge centred at and including a single pier. Bruce and Croasdale (2001) assumed that the tilt recorded at the Pier 31 tiltmeters was proportional to the square of the wind speed measured at an anemometer located on the bridge deck close to Pier 31

$$\overline{T} = k\overline{V}^2 \tag{2}$$

where $\overline{T}$ is the mean pier tilt at water level in μRad; $\overline{k}$ is an empirically derived calibration factor that represents the effective drag coefficient; geometric properties and stiffnesses of the bridge superstructure, and $\overline{V}$ is the transverse component of the ten-minute mean wind velocity in m/s at the anemometer height.

To estimate the static drag coefficients for the bridge deck, Eq. (2) is normalized using the reference wind velocity pressure, q, where

$$q = \frac{1}{2}\rho\overline{V}^2 \tag{3}$$

and ρ is the air density. Using Eqs. (2) and (3), the normalized mean pier tilt can be expressed as

$$\frac{\overline{T}}{q} = \frac{2k}{\rho} \tag{4}$$

For k = 0.25 (μRad - sec^2/m^2) (Bruce and Croasdale 2001) and ρ = 1.25 (kg/m^3), the normalized mean pier tilt is

$$\frac{\overline{T}}{q} = 0.4\ \mu\text{Rad/Pa} \tag{4a}$$

To assess the effective drag coefficient at midspan, it is assumed that the relative magnitude of the drag coefficient for different depths of the superstructure is accurately represented by the 1994 section model tests. Normalized values of the static drag coefficients, that vary with the depth of the superstructure, are determined by a regression analysis of experimental data for the girder section at midspan, the quarter point, the cantilever tip and pier face, as determined from the 1994 wind tunnel study. The fit has the form

$$C'_d = a\,D^b + c \tag{5}$$

where C'_d is the drag coefficient normalized with respect to the static drag coefficient, C_d, at midspan; D is the concrete box girder depth in m; and a, b, and c are parameters estimated by regression analysis. Regression analysis yields

$$C'_d = 0.138\,D^{1.23} + 0.123 \tag{5a}$$

The fit, shown in Fig. 2, is excellent. Using Eq. (5(a)), the drag coefficients for the continuous span and two cantilevers, including two half drop-in spans, were then normalized by dividing the drag coefficient at the 4.5 m deep midspan section as shown in Fig. 3. The normalized drag coefficient, $C_{d(x)}$, has a maximum value of 3.62 at the piers and reduces to 1.0 at midspan as shown.

For each node of the numerical model, the normalized static force, F'_d, was calculated as

$$F'_d = C'_d\,q'\,B \tag{6}$$

where q' is a unit wind pressure of 1 Pa, and B is the width of the bridge deck (or pier) in metres.

Using Eq. (6), each node of the numerical bridge model (Bakht 2010) was loaded with the normalized static force, F'_d, that varied along the bridge length in proportion to the normalized drag coefficients shown in Fig. 3.

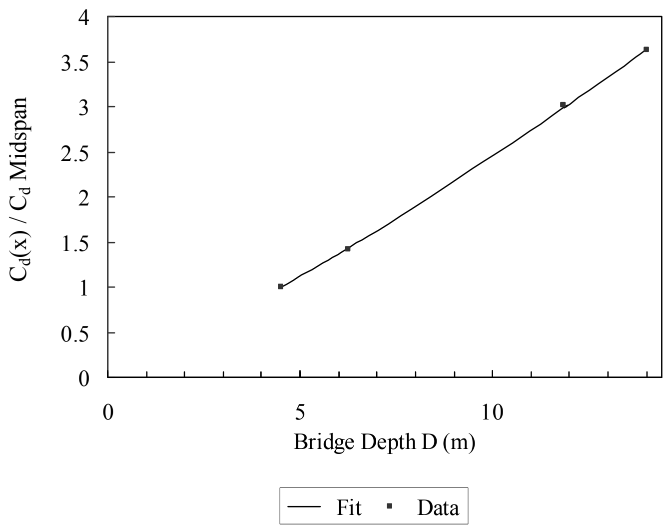

Fig. 2 Variation of Normalized Drag Coefficient with Section Depth

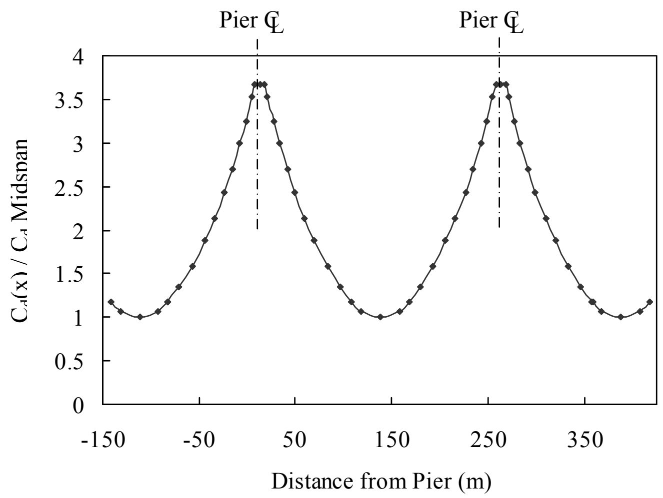

Fig. 3 Variation of Normalized Drag Coefficient for the Continuous Span and Two Cantilevers

Static analysis was carried out and the normalized mean pier tilt at the water level was determined to be

$$\frac{\overline{T}'}{C_d' q'} = 0.69\ \mu\text{Rad/Pa} \tag{7}$$

Using Eqs. (4) and (7) the effective drag coefficient at midspan can be determined as

Table 1 Drag Coefficients – 1994 Design Criteria versus On-Site Monitoring

Location	Drag Coefficients		Average Difference
	1994 Design Criteria	On-Site Monitoring	
Midpoint of Continuous Span	0.58	0.58	0.63 %
Cantilever Tip	0.82	0.83	
Quarter-Point of Continuous Span	1.75	1.76	
Pier Face	2.1	2.11	

$$C_d = \frac{\overline{T}}{q} \Big/ \frac{\overline{T}'}{C_d' q'} \tag{8}$$

From Eqs. (4(a)) and (7), Eq. (8) yields C_d = 0.58. This value is compared to the static drag coefficient used for design in Table 1. The horizontal drag coefficients from the 1994 wind-tunnel investigation used to design the bridge are within 1% of those determined using the on-site monitoring data.

2.2 Dynamic wind loads

The dynamic wind load contribution due to oscillation in the jth natural mode in the loading model originally proposed by King and *et al.* (1994) can be expressed as

$$W_{dyn_j}(x) = \pm q_{ref}\, C_e\, B\, C_{dyn_j}\, a_j(x) \tag{9}$$

where $W_{dyn_j}(x)$ is the j^{th} mode dynamic wind load, with units force/length, that varies with location along the span, x, according to the shape of mode j for a given wind speed as shown in Fig. 1; q_{ref} is the reference velocity pressure at 10 m elevation; C_e is the exposure coefficient; B is the width of the bridge; C_{dyn_j} is the j^{th} mode dynamic load coefficient determined from wind tunnel measurements; and, $a_j(x)$ is the modal load distribution function for mode j, which is the mode shape scaled to have a maximum displacement of 1.0.

To conform to the methodology used in the present study to derive the dynamic wind loads, Eq. (9) can be expressed as

$$W_{dyn_j}(x) = \pm L_j\, a_j(x) \tag{10}$$

where L_j is the "maximum modal load", i.e., the magnitude of the maximum dynamic wind load, with units force/length, in mode j for a given wind speed. Comparing Eqs. (9) and (10)

$$L_j = \pm q_{ref}\, C_e\, B\, C_{dyn_j} \tag{11}$$

Investigation of the acceleration power spectra at different bridge locations has shown that the fundamental modes of vibration contain more than 95% of the energy and the contribution of non-resonant background response is less than 5% (Bakht 2010). Given this absence of non-resonant background response, the total dynamic response, R_{t_d}, in Eq. (1) can be represented by the resonant components as a root-sum-of-squares

$$R_{t_d} \cong \sqrt{\sum_j R_{r_j}^2} \tag{12}$$

Thus the total and modal responses, R_{t_d} and R_{r_j}, respectively, determined from the power spectra in the companion paper can be used to compute the equivalent dynamic wind loads. Table 2 summarizes results of the on-site monitoring data analysis from the companion paper used to compute maximum modal loads, L_j, for the design wind speed of 30.5 m/s approaching from “bridge north”, i.e., at right angles to the bridge alignment. The chosen wind speed is also coincidently the maximum wind speed normal to the bridge axis observed during the November 2001 wind storm which was a near-specified design event as discussed in the companion paper. The regression parameters β and α characterize the normalized modal displacement, Δ_{nj}, as a function of the reduced velocity, $V^*(=V/f_jB)$, as

$$\Delta_{n_j} = \beta\left(V_j^*\right)^{\alpha} \tag{13}$$

Four transverse and three vertical resonant modes of vibration are identified from the power spectra of acceleration. Fig. 4 shows the unit modal load distribution functions, $a_j(x)$, (i.e., normalized mode shapes with a unit maximum ordinate) obtained using a three-dimensional frame analysis model of the bridge, each of which corresponds to one of the significant observed modes of vibration in the prototype responses. The static analysis for each load case yields a set of modal displacement coefficients, $I_j(x)$, defined as the displacement at deck location x, due to the application of the unit modal load distribution functions. The ratio of the maximum modal displacement for a given wind velocity to the maximum modal displacement coefficient gives the maximum modal load, L_j, with units [force/length],:

Table 2 Derivation of Dynamic Wind Loads Using On-Site Monitoring Data

On-Site Monitoring Data	Wind Speed V (m/s)	30.5						
	Wind Azimuth	Bridge North						
	Direction	Transverse				Vertical		
	β	1.34×10^{-6}				6.60×10^{-6}		
	α	3.06				2.94		
	Mode Shape	TS1	TA1	TS2	TA2	VA1	VS1	VS2
	Frequency f_j (Hz)	0.343	0.397	0.485	0.913	0.57	0.678	0.942
Derivation	$\Delta_{nj}B$ $\times 10^{-3}$ (m)	7.39	4.72	2.56	0.37	6.42	3.85	1.46
	$\max(I_j)$ $\times 10^{-6}$ m/(N/m)	6.59	5.04	3.61	1.38	2.64	1.83	0.80
	L_j (kN/m)	1.12	0.94	0.71	0.27	2.43	2.10	1.83

$$L_j = \frac{\Delta_{n_j} B}{\max\ (I_j)} \tag{14}$$

The resulting maximum modal loads are shown in Table 2 for four transverse and three vertical modal load distributions. The maximum modal loads are used to determine the modal response at critical bridge locations and are summed as root sum of squares to obtain the total dynamic response.

3. Wind loads from model-scale bridge data

Several modifications to the 1994 bridge model were made before the 2009 wind tunnel testing which are described in detail in Bakht (2010). Following the procedure described above, the dynamic wind loads were computed using 2009 wind tunnel test data for a mean full-scale wind speed of 30.5 m/s normal to the bridge axis. The salient results are summarized in Table 3. The maximum modal loads, L_j, were computed, which are appropriate for the as-tested model damping.

Davenport (1981) has shown that the resonant response is inversely proportional to the square root of total damping, which is the sum of structural and aerodynamic damping. The structural damping is constant for each mode; however, aerodynamic damping varies with reduced velocity. For simplicity, a representative value of reduced velocity corresponding to the design wind speed of 30.5 m/s was chosen to compute the damping correction for the maximum modal loads. Thus, the maximum modal loads that would be expected given the actual prototype damping, L_{cj}, can be expressed as

Table 3 Derivation of Dynamic Wind Loads Using 2009 Wind Tunnel Test Data

'09 Wind Tunnel Data	Wind Speed V (m/s)	30.5						
	Wind Azimuth	Bridge North						
	Direction	Transverse				Vertical		
	β	1.027×10^{-5}				1.095×10^{-5}		
	α	2.3				2.9		
	Mode Shape	TS1	TA1	TS2	TA2	VA1	VS1	VS2
	Frequency f_j (Hz)	9.37	12.16	16.11	29.13	15.59	17.96	20.59
Derivation	$\Delta_{nj} B \times 10^{-3}$ (m)	12.35	6.78	3.55	0.91	10.03	6.65	4.48
	$\max(I_j) \times 10^{-6}$ m/(N/m)	6.75	3.86	2.44	0.58	2.13	1.88	1.53
	L_j (kN/m)	1.83	1.76	1.46	1.57	4.71	3.54	2.92
	ζ_{tm_j} (%)	0.63	0.52	0.52	0.25	0.92	0.76	0.6
	ζ_{tp_j} (%)	2.0	1.95	1.68	1.95	3.91	2.06	1.51
	L_{c_j} (kN/m)	1.02	0.91	0.81	0.56	2.29	2.15	1.84

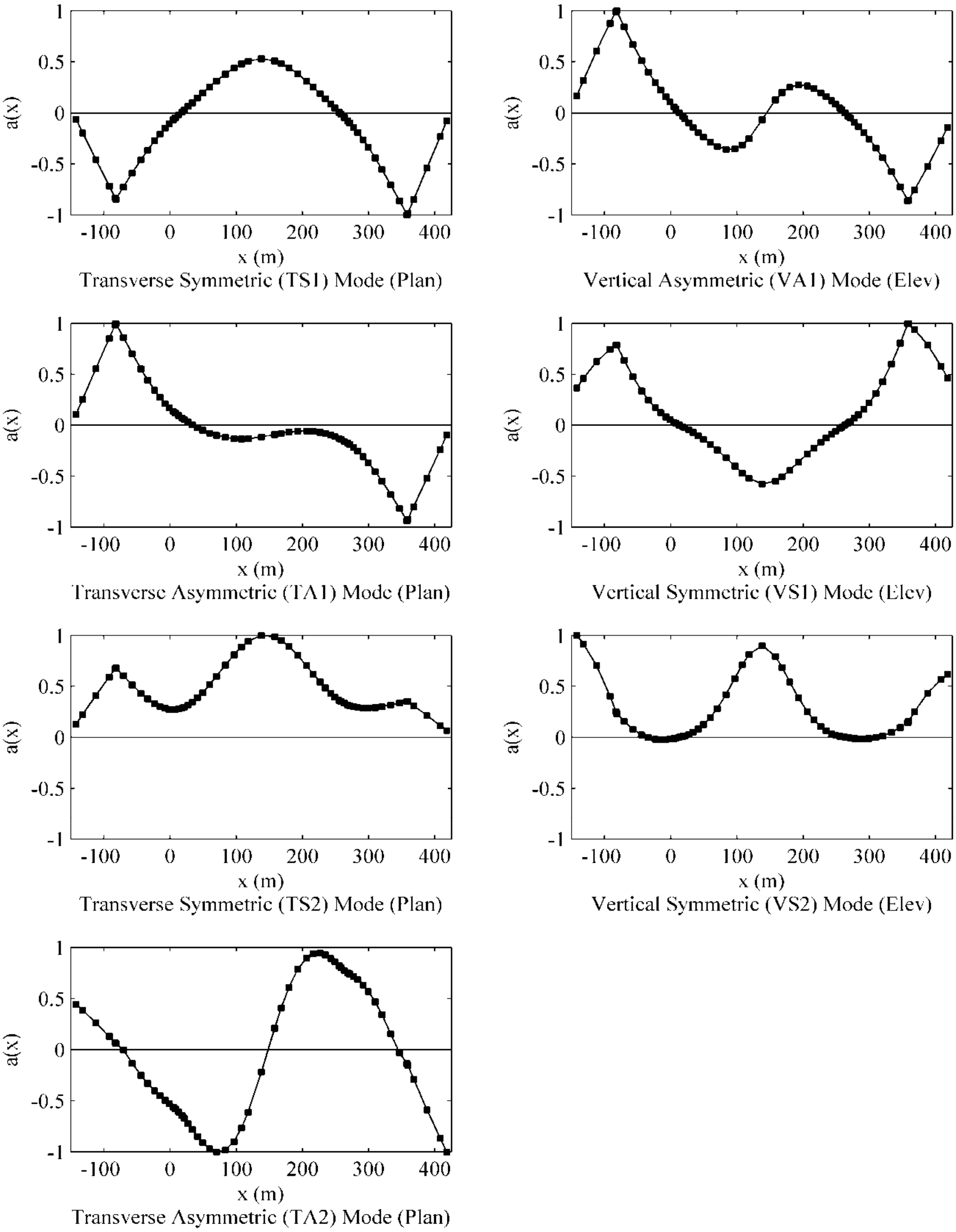

Fig. 4 Prototype Modal Load Distribution Functions for the Transverse and Vertical Mode Shapes

$$L_{c\,j} = L_j \frac{\sqrt{\zeta_{tm_j}}}{\sqrt{\zeta_{tp_j}}} \tag{15}$$

where: ζ_{tm_j} is the j^{th} mode total damping for the model (structural plus aerodynamic); and ζ_{tp_j} is the j^{th} mode total damping for the prototype (structural plus aerodynamic).The estimated values of ζ_{tm_j} and ζ_{tp_j} are shown in Table 3. Using Eq. (15), a damping correction is applied to each maximum modal load and the resulting, L_{c_j} , values are also shown in Table 3. These corrected loads will be used to predict the equivalent full-scale bridge response for comparison to the responses predicted using loads derived from the on-site monitoring data and the 1994 wind tunnel test results.

4. Comparison of Responses

In this section, the full-scale observed RMS accelerations are compared to the equivalent full-scale RMS accelerations predicted using 2009 and 1994 wind tunnel loads. Bending moments are critical for the bridge design, therefore, RMS and peak bending moments predicted using loads derived from the on-site monitoring data and the wind tunnel tests will also be compared.

4.1 RMS accelerations

Fig. 5 compares RMS accelerations measured at the prototype to those predicted from the

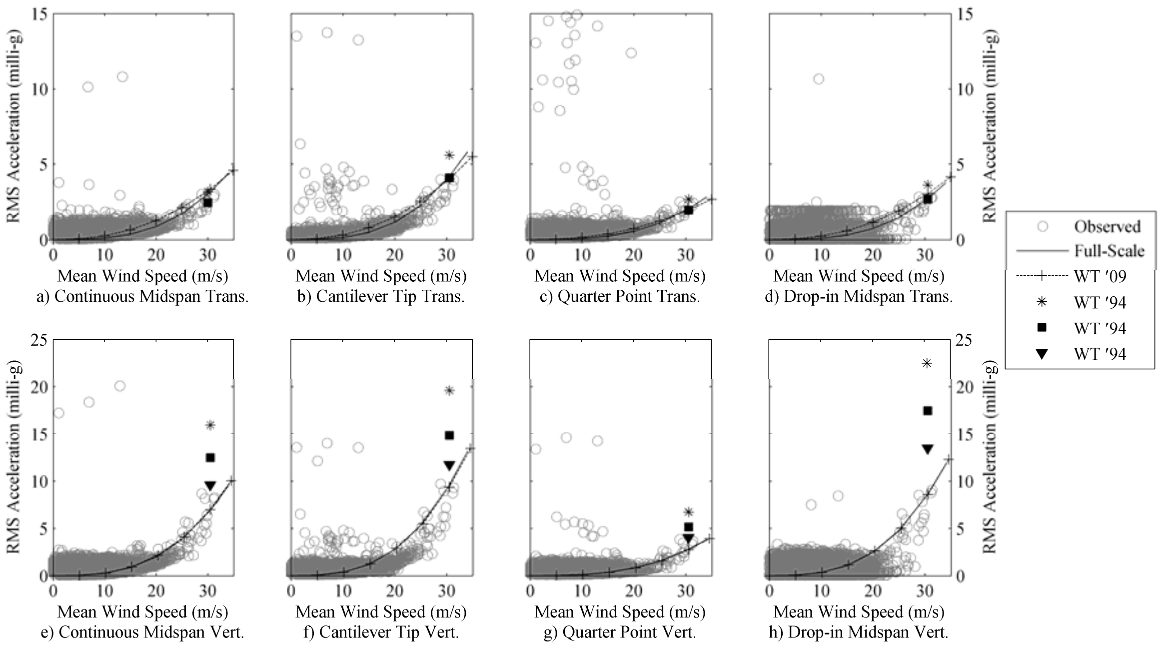

Fig. 5 Observed and Predicted RMS Accelerations Using Loads Derived from the On-Site Monitoring Data and the 2009 and 1994 Wind Tunnel Test Results

wind-tunnel-based loadings. The horizontal axis of each figure is the full-scale wind speed, and the vertical axes are the Root-Mean-Square (RMS) accelerations. Figs. 5(a) to (d) show transverse accelerations at the midspan of the continuous span (see Fig. 5 of the companion paper), the cantilever tip, the quarter point of the continuous span, and the mid span of the drop-in span, respectively, and Figs. 5(e) to (h) show the vertical accelerations at these locations. The open circles are the RMS accelerations derived from the on-site monitoring data. Large RMS accelerations for wind speeds below 15 m/s were examined for the signs of potential vortex shedding-induced vibration. In all cases the peak factors of the responses (i.e. the ratio of the peak to the RMS acceleration) were in the range of 3 to 5, which is typical of random response. Sinusoidal response as would be the case with vortex shedding excitation is typically characterized by low peak factors of the order of $\sqrt{2}$, which is the maximum/RMS of a sinusoidal signal. Therefore, it is believed that most of these events were related to heavy truck traffic and not wind loading. The solid lines are the RMS accelerations predicted using loads derived from the on-site monitoring data. The broken lines with markers (+) are the equivalent RMS accelerations predicted using loads derived from the 2009 wind-tunnel test results. Both the solid and broken lines are in excellent agreement at all bridge locations: for the vertical RMS accelerations, the two curves are indistinguishable. The damping estimates for the prototype, available from the on-site monitoring data, play a crucial role in better predicting the equivalent RMS accelerations. The excellent agreement between the full-scale and 2009 wind tunnel responses demonstrates that the proposed methodology can be used to compute wind loads using on-site monitoring or wind-tunnel data.

The impact of the assumed total damping on the wind load estimates can also be quantified. In Fig. 5, the asterisk markers are the RMS accelerations predicted using the original 1994 wind tunnel loads, assuming the damping of the bridge to be 0.63% of critical, used for the bridge design. The solid squares are the RMS accelerations predicted using 1994 design loads adjusted to the prototype damping ranging from 1.5% to 3.9% of critical shown in Table 3. The solid squares are in close agreement with the observed values and the 2009 wind tunnel predictions for the transverse RMS accelerations. The vertical RMS accelerations predicted using the 1994 design loads, shown as solid squares, are conservative with respect to the observed values and the 2009 wind tunnel predictions, however, particularly for the two midspans and cantilever locations. This conservatism may be due to a viscous damper attached at the midpoint of the continuous span of the full-aeroelastic model tested in 1994 that was intended to ensure the damping was 0.63% of critical. It is believed that the damper was not effective for full-scale wind speeds less than 32 m/s so using Eq. (15), a further damping correction was applied to the VS1 modal load. The corresponding vertical RMS accelerations, shown as inverted solid triangles in Fig. 5, lie above the observed and 2009 wind tunnel vertical RMS accelerations, indicating the loads predicted from the 1994 study are still conservative, but markedly less so.

5. Bending moments

5.1 RMS bending moments

The loads derived from the on-site monitoring data, the 2009 wind tunnel test data, and the 1994 wind tunnel test data using two damping values were used to predict RMS bending moments at midspan and pier faces for the prototype for further comparison. Fig. 6 compares these bending

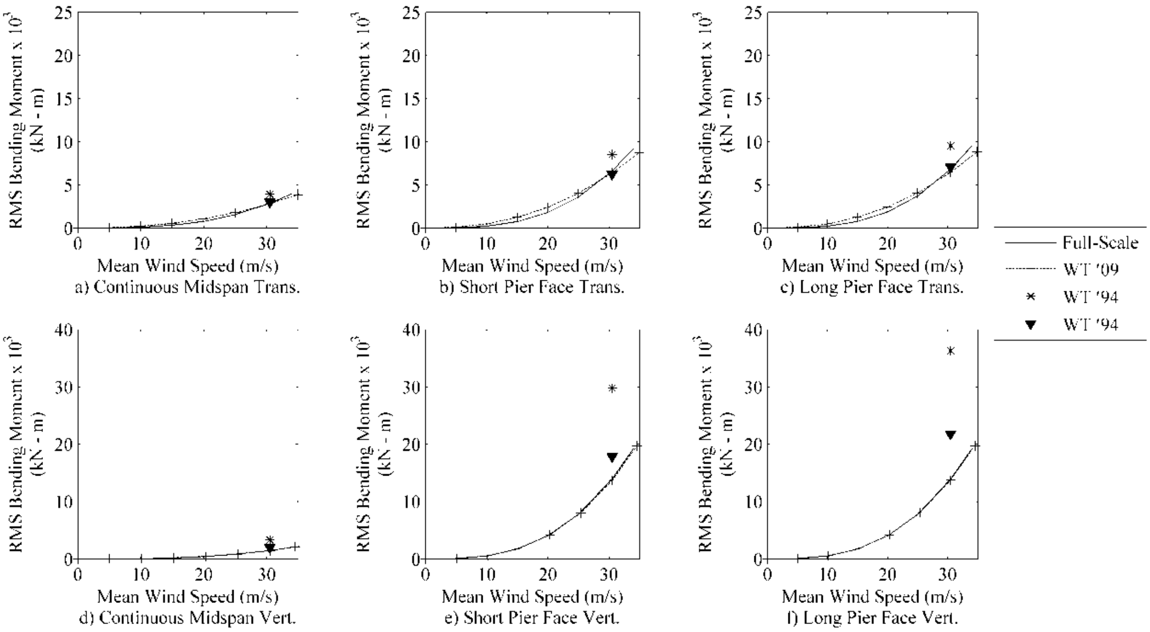

Fig. 6 Predicted RMS Bending Moments Using Loads Derived from the On-Site Monitoring Data and the 2009 and 1994 Wind Tunnel Test Results

moments, in the transverse and vertical directions, at the midpoint of the continuous span and two pier faces with 21.7 m and 29.3 m pier depths below water, termed as short and long pier faces, respectively. The solid lines are the RMS moments predicted using loads determined from the on-site monitoring data. The broken lines with markers are the RMS moments predicted using 2009 wind tunnel loads. The asterisks are the RMS moments based on the 1994 wind tunnel loads adjusted to 0.63% damping used for the bridge design. The inverted triangles are the RMS moments predicted using 1994 design loads corrected to the prototype damping ranging from 1.5% to 3.9% of critical shown in Table 3. For the damping correction, the 1994 design loads were considered to have 0.63% damping except for mode VS1, which was assumed to have 0.15% damping for wind speeds less than 32 m/s as described in the discussion of Fig. 5.

The transverse RMS moments predicted using loads derived from the on-site monitoring data and the 2009 wind tunnel model test results agree very well as shown in Figs. 6 (a), (b) and (c). The agreement for the vertical RMS moments, Figs. 6 (d), (e) and (f) is excellent: the curves lie on top of each other. The asterisks indicate that the vertical RMS moments predicted using the 1994 design loads are conservative with respect to the loads derived from the on-site monitoring data and the 2009 wind tunnel test results, whereas the transverse RMS moments are in better agreement. The inverted triangles indicate that the transverse RMS moments predicted using 1994 design loads corrected to the prototype damping are in good agreement with the RMS moments predicted using loads derived from the on-site monitoring data and the 2009 wind tunnel test results; however, the vertical RMS moments are conservative.

Table 4 compares RMS moments predicted for a mean wind speed of 30.5 m/s using loads derived from the on-site monitoring data and from the 2009 and 1994 wind tunnel investigations. The derived loads from the on-site monitoring data and the 2009 wind tunnel test results are based

Table 4 Comparison of RMS Bending Moments for Mean Wind Speed 30.5 m/s Normal to the Bridge Axis

(a) Transverse Loads and Bending Moments

Data Type	Modal Wind Loads (kN/m)				Root Mean Square (RMS) Bending Moment (kN-m × 10^3)			RMS Bending Moment Ratio with respect to Full-Scale		
	TS1	TA1	TS2	TA2	Mid-span	Long Pier Face	Short Pier Face	Mid-span	Long Pier Face	Short Pier Face
On-Site Monitoring	1.12	0.94	0.71	0.27	2.87	6.62	6.81	1.00	1.00	1.00
Wind Tunnel '09	1.02	0.91	0.81	0.56	2.81	6.43	6.45	0.98	0.97	0.95
Wind Tunnel '94[1]	1.78	1.08	-	-	3.91	8.54	9.53	1.37	1.29	1.40
Wind Tunnel '94[2]	1.34	0.73	-	-	2.94	6.21	6.99	1.03	0.94	1.03

(b) Vertical Loads and Bending Moments

Data Type	Modal Wind Loads (kN/m)				Root Mean Square (RMS) Bending Moment (kN-m × 10^3)			RMS Bending Moment Ratio with respect to Full-Scale		
	VA1	VS1	VS2	VA2	Mid-span	Long Pier Face	Short Pier Face	Mid-span	Long Face	Short Face
On-Site Monitoring	2.43	2.10	1.83	-	1.46	13.99	13.91	1.00	1.00	1.00
Wind Tunnel '09	2.29	2.15	1.84	-	1.49	13.63	13.74	1.01	0.97	0.99
Wind Tunnel '94[1]	2.3	7.5	-	-	3.33	29.74	36.28	2.28	2.13	2.61
Wind Tunnel '94[2]	1.33	4.56	-	-	2.02	17.95	21.96	1.38	1.28	1.58

[1] recommended wind loads based on 1994 wind tunnel testing with an assumed 0.63% damping
[2] 1994 wind tunnel loads adjusted to prototype damping

on four transverse and three vertical modal loads each. The 1994 wind tunnel loads considered only two modal loads in each direction, which were based on the energy contained in the spectral peaks for these modes and found to be sufficient to develop the observed responses.

The values shown in the three columns at the right side of Table 4 are the RMS moments predicted using the various wind tunnel loads normalized using the RMS moments derived from the on-site monitoring data. The transverse and vertical RMS moments predicted using the 2009 wind tunnel loads are within 5% of the values derived from the on-site monitoring data. The transverse and vertical RMS moments predicted using the 1994 design loads assuming 0.63% damping are within 40% and 161% of the on-site monitoring values respectively. In the absence of realistic estimates of the prototype damping, the designer always uses a conservative value. If the 1994 design loads are adjusted to realistic prototype damping the resulting transverse RMS moments are within 6% and the vertical RMS moments are between 28% - 58% of the RMS moments derived from the on-site monitoring data. Thus the knowledge of prototype damping is essential for accurately estimating dynamic wind loads based on wind tunnel tests.

5.2 Peak bending moments

Peak bending moments are the maximum values of the static bending moment and the peak dynamic bending moment. Table 5 compares peak bending moments predicted using loads derived from the on-site monitoring data and the 2009 wind tunnel test results for a mean wind speed of 30.5 m/s normal to the bridge axis, as occurred during the November 2001 storm, with the peak bending moments predicted using the design loads specified in 1994. The mean bending moments are the static moments obtained using the 2009 wind tunnel test results as they were readily available. The dynamic wind loads from the on-site monitoring data are used to determine RMS bending moments. A mean peak factor of 3.47 was determined from the analysis of the on-site monitoring data (Bakht 2010). Using Eq. (1), peak bending moments are computed for the transverse and vertical directions.

Table 5 Comparison of Peak Bending Moments Predicted for a Mean Wind Speed of 30.5 m/s Normal to the Bridge Axis

(a) Transverse

Load Type	Mean Bending Moment (kN-m × 10^3)			RMS Bending Moment (kN-m × 10^3)			Peak Bending Moment (kN-m × 10^3)		
	Mid-span	Short Pier Face	Long Pier Face	Mid-span	Short Pier Face	Long Pier Face	Mid-span	Short Pier Face	Long Pier Face
Wind Tunnel '09[1] On-Site Monitoring[2]	8.94	38.15	38.15	2.87	6.62	6.81	18.97	61.31	61.98
Design Loads	8.81	37.88	37.88	3.91	8.54	9.53	22.51	67.79	71.23
Ratio – Design / (WT '09 or On-Site)	0.98	0.99	0.99	1.36	1.29	1.40	1.19	1.11	1.15

(b) Vertical

Load Type	Mean Bending Moment (kN-m × 10^3)			RMS Bending Moment (kN-m × 10^3)			Peak Bending Moment (kN-m × 10^3)		
	Mid-span	Short Pier Face	Long Pier Face	Mid-span	Short Pier Face	Long Pier Face	Mid-span	Short Pier Face	Long Pier Face
Wind Tunnel '09[1] On-Site Monitoring[2]	2.97	30.66	30.66	1.46	13.99	13.91	8.09	79.64	79.34
Design Loads	3.19	28.85	28.85	3.33	29.74	36.28	14.85	132.94	155.83
Ratio – Design / (WT '09 or On-Site)	1.07	0.94	0.94	2.28	2.13	2.61	1.84	1.67	1.96

[1] Mean Bending Moments correspond to 2009 Wind Tunnel Tests
[2] RMS Bending Moments correspond to On-site Monitoring Data

The force coefficients determined from the section model tests (King *et al*. 1994, JMS 1995) are used to compute design mean bending moments and the dynamic force coefficients determined from the full-aeroelastic model test (King *et al*. 1994, King *et al*. 1995, JMS 1995) are used to compute design RMS bending moments. A peak factor of 3.5 was recommended for the bridge design (King *et al*. 1994). Using Eq. (1) design peak bending moments are computed for the transverse and vertical directions.

The peak bending moments due to the specified design wind loads are 11% – 19% higher in the transverse direction and 67% - 96% higher in the vertical direction compared to the peak bending moments during November 2001 storm. These are specified (i.e., unfactored) values. The higher percentage difference in the vertical peak moments is due to the higher modal damping assumed for mode VS1 for wind speeds less than 32 m/s as described in the discussion of Fig. 5. Hence it can be concluded that the bending moments caused by the passage of November 2001 storm approached, but did not exceed, those corresponding to the specified design wind loads.

6. Conclusions

Full-aeroelastic wind tunnel models are a promising alternative to section models for bridge superstructures with both variable and uniform cross sections to derive design wind loads and assess the wind-induced response. The variable depth of the Confederation Bridge superstructure required wind loads to be predicted in 1994 using, for the first time, a full-aeroelastic model. A decade of on-site monitoring data, analysed in detail in the companion paper, has been used to derive, for the first time, the wind loads that the structure has been subjected to. Comparison of these loads and associated bending moments with those predicted in 1994 and 2009 wind tunnel tests of the full-aeroelastic model facilitates validation of the methodology and highlights the need to predict the prototype damping accurately to obtain realistic loading estimates.

The following conclusions are drawn:

1. The static drag coefficients developed using on-site monitoring tiltmeter data are within 1% of those used for the bridge design thus validating the 1994 wind tunnel test results.
2. The dynamic load effects predicted using 2009 wind tunnel loads are within 5% of the values predicted using loads from the on-site monitoring data. This excellent agreement validates the methodology used for the derivation of dynamic wind loads using aeroelastic model tests.
3. The transverse and vertical dynamic load effects predicted using 1994 wind tunnel loads used for the bridge design, are 40% and 161% greater than the values predicted using loads from the on-site monitoring data, respectively. The 1994 wind tunnel predictions are conservative, especially in the vertical direction, because the damping of the prototype was conservatively assumed to be 0.13 to 0.63 % of critical, whereas the on-site monitoring data indicate it to be 1.51 to 3.91 % of critical. When modified to reflect the observed prototype damping the predicted load effects are 6% and 58% greater than the load effects derived from the on-site monitoring data in the transverse and vertical directions, respectively.
4. The dynamic load effects predicted using 1994 design loads modified to reflect the observed prototype damping are 6% greater in the transverse direction and 28% -58% greater in the vertical direction than the load effects derived from the on-site monitoring data.
5. For the specified mean 10-minute wind speed of 30.5 m/s normal to the bridge, the maximum bending moments due to the specified (i.e. unfactored) loads for the bridge design in 1994 are 11% - 19% greater in the transverse direction and 67% - 96% greater in the vertical direction than those

induced during the November 2001 storm experiencing the same wind speed. The bridge has not been therefore subjected to its specified (i.e., unfactored) wind force effects between 1998 and 2006, even during the November 2001 storm.
6. The present study demonstrates that only a small number of dominant modes are required to accurately capture the wind loads and their effects.

Acknowledgments

The authors would like to thank Strait Crossing Bridge Limited for providing on-site monitoring data and sponsoring scholarship applications to Natural Sciences and Engineering Research Council (NSERC) of Canada, and Mathematics of Information Technology and Complex Systems (MITACS). The generous funding through various sources including NSERC, MITACS, Western Engineering Scholarship, Western Graduate Research Scholarship, Alan G. Davenport Award and Graduate Thesis Research Awards Fund is greatly acknowledged.

References

AASHTO 2004. *AASHTO LRFD Bridge Design Specification,* American Association of State Highway and Transportation Officials, Washington, USA.

Bakht, B. (2010), *Assessment of Wind Induced Response and Drivability of the Confederation Bridge,* Ph.D. Thesis, Department of Civil and Environmental Engineering, University of Western Ontario.

British Standard Institute (BSI) (2009), *Design Manual for Roads and Bridges,* BD 37/01 Volume 1, Section 3, Part 14, Loads for Highway Bridges. BS 5400. British Standard Institution London.

Brown, T.G. (2007), Ice Force Monitoring, *Confederation Bridge Engineering Summit Proceedings,* Charlottetown, PEI, Canada, pp. 224-254.

Bruce, J.R. and Croasdale, K.R. (2001), *Confederation Bridge Ice Force Monitoring Joint Industry Project Annual Report,* IFN Engineering Ltd. Report Number 00-1-001, 40p.

Canadian Standards Association (CSA) (2006), *Canadian Highway Bridge Design Code (CHBDC). A National Standard of Canada,* Canadian Standards Association CAN/CSA – S6 – 06. Canadian Standards Association, Toronto, Canada.

Davenport, A.G. (1964), “Note on the distribution of the largest value of a random function with application to gust loading”, *Proceedings of the Institution of Civil Engineers,* Paper No. 6739, Vol. 28, 187-196.

Davenport, A.G. (1979), “The influence of turbulence on the aeroelastic responses of tall structures to wind”, *IAHR/IUTAM Symposium,* Karlsruhe, Germany, pp. 681-695.

Davenport, A.G. (1981), “Reliability of long span bridges under wind loading”, *Proceedings of the 3rd International Conference on Structural Safety and Reliability (ICOSSAR)*, Norway.

Davenport, A.G. and King, J.P.C. (1984), “Dynamic wind forces on long span bridges”, *Proceedings of the 12th IABSE Congress,* Vancouver, Canada.

Davenport, A.G. (1988), “The response of tension structures to turbulent wind: the role of aerodynamic damping”, *Proceedings of the 1st International Oleg Kerensky Memorial Conference on Tension Structures,* London, England.

JMS. (1995), *Design Criteria, Northumberland Strait Crossing Project, Revision 7.0.*, Jean Muller International, Stanley Joint Venture Inc., Calgary, Alberta.

King, J.P.C., Mikitiuk, M.J., Davenport, A.G. and Isyumov, N. (1994), *A Study of Wind Effects for the Northumberland Straits Crossing,* BLWT-SS8-1994, Boundary Layer Wind Tunnel Laboratory, University of Western Ontario (Parts of this report have been published in King and Davenport 1994b and King 1999).

King, J.P.C. and Davenport, A.G. (1994), "P.E.I. fixed link – the treatment of wind effects for the Northumberland Strait Crossing", *Proceedings of the 4th International Conference on Short and Medium Span Bridges,* Halifax, Nova Scotia, Canada.

King, J.P.C., Crooks, G.J. and Davenport, A.G. (1995), *The Northumberland Straits Crossing, Prince Edward Island Testing of Marine Span Aeroelastic Model and Analysis of Dynamic Wind Loads,* BLWT-SS24-1995, Boundary Layer Wind Tunnel Laboratory, University of Western Ontario.

King, J.P.C. (1999), "Integrating wind tunnel tests of full-aeroelastic models into the design of long span bridges", *Proceedings of the 10th International Conference on Wind Engineering (ICWE),* Copenhagen, Denmark.

Scanlan, R.H. (1987), "Interpreting aeroelastic models of cable-stayed bridges", *J. Eng. Mech. - ASCE,* **113**(4), 555 - 575.

CC